International Conference on Space Optics—ICSO 2022

Dubrovnik, Croatia

3–7 October 2022

Edited by Kyriaki Minoglou, Nikos Karafolas, and Bruno Cugny,

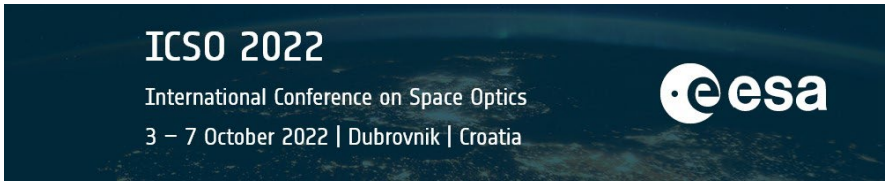

Microwave Photonic filter with reconfigurable bandwidth and tunable central frequency aimed for flexible satellite payloads in Ka-, Q-, -V band

International Conference on Space Optics — ICSO 2022, edited by Kyriaki Minoglou, Nikos Karafolas, Bruno Cugny, Proc. of SPIE Vol. 12777, 127774Z · © 2023 ESA and CNES · 0277-786X · doi: 10.1117/12.2690897

Microwave Photonic filter with reconfigurable bandwidth and tunable central frequency aimed for flexible satellite payloads in Ka-, Q-, -V band

Charoula Mitsolidou*[a], Roelof Bernardus Timens[a], Víctor Sánchez-Martínez[b], Alberto Zarzuelo[c], Guillermo Carpintero[c], Peter D. H. Maat[a], Paulus W. L. van Dijk[a], Chris G. H. Roeloffzen[a]
[a]LioniX International BV, Hengelosestraat 500, 7521 AN, Enschede, The Netherlands; [b]SENER Aeroespacial S.A., Severo Ochoa 4, 28760 Tres Cantos, Spain, [c]Universidad Carlos III de Madrid, Av. de la Universidad, 30, 28911 Leganés, Spain

ABSTRACT

We propose a microwave photonic band-pass filter in the TriPleX® waveguide technology, capable of performing channel selection in flexible DEMUX satellite systems. The proposed channel selector consists of 2 stages of filtering, that enable fully reconfigurable central frequency and channel bandwidth tuning in the Ka-, Q- and V-band. The first stage of filtering is based on a Coupled Ring Optical Waveguide (CROW) filter and serves as channel bandwidth regulator. The CROW filter includes 8 ring resonators, each with a length of 7.38 cm, corresponding to a Free Spectral Range (FSR) of 2.6667 GHz. Bandwidth reconfigurability is achieved by using ultra low-loss, stress-optic lead zirconate titanate (PZT)-based tunable couplers between the ring resonators, while central frequency tunability is enabled for the whole Ka-band by incorporating a tunable PZT-based phase shift on each ring resonator. The second stage of filtering consists of Asymmetric Mach-Zehnder Interferometer (AMZI) - lattice filters and serves as FSR extender. AMZI lattice filters with FSR of 5.3334 GHz and 10.6668 GHz, respectively, are used to expand the central frequency tunability of the channel selector in the Q- and V-band. The lattice filters are also equipped with tunable phase shifters to allow for tunability in the central frequency. The proposed 2-stage channel selector filter has a f_{FSR}=10.6668 GHz and exhibits a tunable passband bandwidth from 125 MHz to 1000 MHz. The passband insertion loss and group delay variation are < 0.9 dB and 2.8 ns, while channel isolation is higher than 50 dB.

Keywords: AMZI, band-pass filter, channel selector, CROW, integrated optics, microwave photonic filter, optical ring resonator, reconfigurable payload

1. INTRODUCTION

Nowadays, satellite telecommunications experience a huge demand for flexible payloads. Such payloads can be enabled through channelization techniques that support dynamic allocation of the available spectral resources. The filter performing the channelization is named channel selector and its main functionality is to separate closely packed channels received at the antenna without introducing appreciable signal distortion. Critical features for the channel selector is the high reconfigurability in bandwidth (BW) and the ability to operate in broad and high frequency spectral bands, such as the Ka-, Q- and V- band. However, realizing these performance in the RF domain is problematic, since the current RF filters present limitations in the maximum operational frequency, the central frequency tunability and BW adjustability.

Microwave photonics (MWP) is an emerging technology that can overcome these fundamental limitations of the current electronics by processing RF signals in the optical domain [1]. MWP technology exhibit significant advantages, such as a broad bandwidth, modulation format transparency, immunity against electromagnetic interferences (EMI) and system reconfigurability [2]. Recently, the implementation of MWP systems by means of photonic integrated circuits (PIC) has resulted on the integrated microwave photonics (iMWP) technology [3]. iMWP systems present all the advantages of the photonics-enabled approach, while in addition they exhibit reduced size, weight, and power consumption, as well as enhanced stability. This establishes a robust hardware platform that can be highly attractive for the realization of compact fully-reconfigurable channel selector filters.

Various MWP RF filters have been demonstrated using different concepts such as non-linear Brillouin Scattering [4], [5], dense wavelength division multiplexing by means of an optical comb [6] and Subwavelength-gratings [7], [8].

However, those approaches are not suitable for satellite applications, since mostly they are based on bulky discrete components and they face limitations in terms of scalability (number of channels), spectral resolution and power consumption. Another common scheme to implement MWP filters are tapped delay-line filters based on Asymmetric Mach Zehnder Interferometers (AMZIs), optical Ring Resonator (RR) structures and their combination [9]-[12]. These filters are easily implemented on iMWP platforms as all its elements (waveguides, directional couplers, phase shifters, and ring resonators) are building blocks of standard design libraries. Among them, the ring resonator based filters are the most attractive choice for dense channelization due to their unique ability to provide MHz-band frequency selectivity in combination with high stopband rejection and large Free Spectral Range (FSR). Previously, we have reported on a high-Q channel selector filter implemented in the Si_3N_4/SiO_2 TriPleX® iMWP platform [13], which is based on a 8 integrated Coupled Resonator Optical Waveguide (CROW) circuitry [14]. The filter is fully tunable within its FSR of 1.4 GHz and exhibits remarkable performance with a 3-dB passband of 72 MHz and a stopband rejection of 51 dB. However, due to the fact that the FSR of the filter is smaller than the BW of the Ka (27.5-30 GHz, BW=2.5 GHz), Q (37.5-42.5 GHz, BW=5 GHz) and V (42.5-50 GHz, BW=7.5 GHz) bands, its reconfigurability within these bands is limited.

Here, we extend our previous work and we propose an iMWP channel selector filter with much larger FSR equal to 10.6668 GHz, capable of demultiplexing independently RF payloads in the whole Ka-, Q- and V-band. The filter consists of 2 stages of filtering: The 1st stage of filtering is based on a CROW filter and serves as channel BW regulator. The CROW filter includes 8 RRs, each with a length of 7.38 cm, corresponding to a $f_{FSRCROW} = 2.667$ GHz. The channel bandwidth depends solely on the inter-resonator coupling strength, which can be programmed through ultra low-power stress-optic lead zirconate titanate (PZT) tunable coupling elements (<1 μW) [15], allowing for selection of the passband bandwidth independently of the RF center frequency. Central frequency tunability for the whole Ka-band is achieved by incorporating tunable PZT-based phase shifts on the ring resonators. The 2nd stage of filtering consists of AMZI-lattice filters and serves as FSR extender. The AMZI lattice filters are used to expand the central frequency tunability of the channel selector in the Q- and V-band. This is achieved through the suppression of parasitic signals that may appear after multiples of the CROW filter's FSR. To this end, the 2nd stage of filtering includes a 2 stage/3 AMZI and a 2 stage/2 AMZI lattice filter with FSR values equal to 5.3334 GHz and 10.6668 GHz, respectively. The filters are equipped by low power consumption stress-optic PZT tuning elements [15] to allow for central frequency reconfigurability.

The channel selector filter exhibits a tunable passband BW that ranges from 125 to 1000 MHz. The passband insertion loss and group delay variation are <0.9 dB and <2.8 ns, respectively, while the channel isolation is > 50 dB. The key to such a performance is the implementation of the channel selector filter on the TriPleX® iMWP platform, which provides a combination of ultra-low loss Si_3N_4/SiO_2 waveguides (<1.5 dB/m) [14], power-efficient tuning elements (<1 μW) [15] and high maturity fabrication of advanced functional circuitries [13].

2. MWP SYSTEM ARCHITECTURE

The MWP filter architecture is shown in Fig. 1. This paper focuses on the photonic-based channel selector filter that forms the demultiplexer (DEMUX). A brief description of the MWP system is given next. A laser produces an optical carrier which is split to 2 paths. One path directs the light through the optical Mach-Zehnder Modulator (MZM), where an incoming RF signal in the Ka-, Q-, or V-band is modulated in a double sideband configuration. Then, the optical signal is taken into an optical Single Side Band –Suppressed Carrier filter (SSBSC). The SSBSC filter eliminates the undesired Lower Side Band (LSB) and the optical carrier, while leaves the signal information in the optical domain in the Upper Side Band (USB). In this stage, the optical-converted USB signal can be considered as a WDM signal that conveys the information of 4 different wavelength channels (λ_1, λ_2, λ_3, λ_4). The USB signal is then processed by the DEMUX channel selector filter, which is responsible for resolving the total BW into 4 separated optical channels. Afterwards, each demultiplexed channel is combined with the Re-injected "clean" optical carrier, emerging from the second output of the 1:2 splitter. Multiplexing of the USB and Carrier signals is performed by the respective Carrier Re-Injection (CRI) filter. Finally, the resulted optical signals are sent to the Photodiode (PD) for optical-to-RF conversion through the beating operation [16].

In this architecture, the main signal processing unit is the channel selector, which performs several important functionalities, such as establishing the bandwidth of the transponder, resolving channels and suppressing adjacent channel interference. Key features of this filter are its ability to provide central frequency tunability and passband bandwidth adjustability, while retaining the spectral response within the required performance.

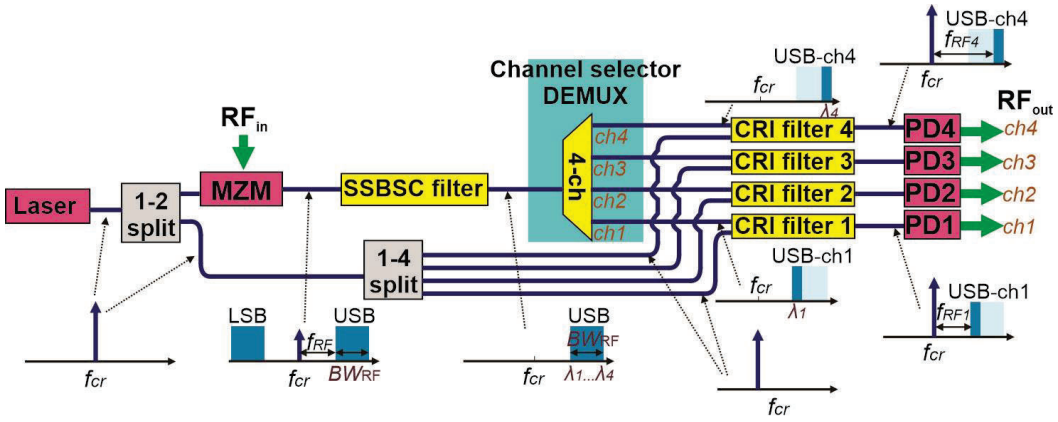

Figure 1. Microwave photonics DEMUX architecture of the proposed channel selector filter.

3. CHANNEL SELECTOR FILTER DESING

Within the ESA contract "Photonic RF Tuneable Demultiplexer for Broadband Satellites-THORMUX", a filter able to provide central frequency tunability simultaneously in Ka-, Q- and V-bands has been designed. To achieve this goal, the filter's FSR must be ≥ BW of the V-band (BW=7.5 GHz) which is the largest BW among the targeted frequency bands. The targeted passband bandwidth adjustability ranges from 125 to 1000 MHz. Flat in-band response with a ripple < 1 dB and group delay variation < 5 ns should be fulfilled simultaneously. Another central requirement is the 40-dB isolation between neighboring channels and the high steepness of the transmission function at the filter edges. Finally, the insertion losses at the central frequency should be as low as possible in order to allow for a high performance MWP link in terms of link gain, noise figure and dynamic range.

The schematic of the proposed single - channel selector filter is depicted in Fig. 2. The first stage of the channel selector is based on the CROW filter with a FSR of 2.6667 GHz ($f_{FSRCROW}$). The FSR has been optimized, so as the filter can be tuned at a BW range of [125 – 1000] MHz, acting as BW regulator. The second stage filtering consists of cascaded AMZI-based lattice filters and is responsible for extending the FSR of the channel selector. Specifically, a 2 stage/ 3 AMZI filter with 2 times the FSR of the CROW is employed ($f_{FSRlatt1}$=5.3334 GHz), followed by another 2 stage/ 2 AMZI filter with 4 times the CROW's FSR ($f_{FSRlatt2}$=10.6668 GHz). The second stage filtering is responsible for suppressing any in-band parasitic signal in Q- and V-bands that may pass through the CROW filter. In this way, the cascade of AMZI-lattice filters extends the FSR of the channel selector to a value equal to 10.6668 GHz, which is larger than the BW of the Ka-, Q- and V-band.

In terms reconfigurability, all AMZI-lattice filters and the CROW filter have tunable central frequency. On the other hand, only the CROW filter has tunable BW to regulate the channel characteristics, while the lattice filters have a fixed BW. The requirement for them is that they need to have large enough stopband bandwidth to suppress unwanted signals, as well as large and flat passband so they do not distort the targeted filter shape for any BW between [125-1000] MHz.

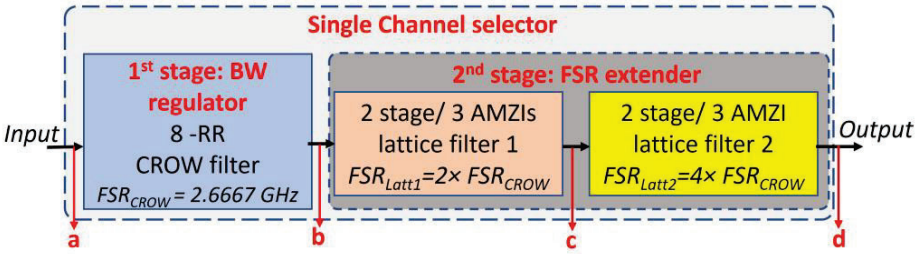

Figure 2. Single-channel selector schematic based on the 2-stage filtering approach.

Fig. 3 presents the functional designs of the individual filters, incorporated in the channel selector chain. Particularly, Fig. 3 (a) depicts the CROW filter design, which is formed by a chain of 8 directly coupled RRs. The adjustable phase shift in the n^{th} RR is donated by φ_n, while κ_n corresponds to the n^{th} tunable power coupling coefficient between the n-1st and n^{th} RR. A number of 17 PZT tuning elements (8 phase shifts, 9 tunable couplers) are employed to allow for filter reconfigurability. With the phase shifters, the central frequency of the filter is controlled, while the tunable power couplers are used for tuning the channel filter characteristics such as power response, group delay responses and passband width. The optimum FSR of the CROW filter found to be equal to $f_{FSRCROW}$ = 2.6667 GHz, which corresponds to a physical circumference of 7.38 cm per ring in Low-Index Contrast Single Stripe (LIC-SS) waveguides with group index (n_{group}) equal to 1.5232 [13]. The FSR has been optimized so as the BW of the passband can range from 125 – 1000 MHz. A major advantage of a CROW filter is that it provides tunable narrow bandwidth with flattop response and high stop-band extinction ratio, making itself the most promising candidate for BW regulation functionality [14].

Fig. 3 (b) and (c) show the proposed AMZI-based lattice filters implementation with FSR equal to 5.3334 GHz ($2\times f_{FSRCROW}$) and 10.6668 GHz ($4\times f_{FSRCROW}$), respectively. The designs consist of 2 filter stages connected as a complementary pair (BAR out for 1st stage /CROSS out for 2nd stage) to allow for at least 50 dB stopband suppression and zero dispersion [17]. Each stage is formed by concatenating AMZIs in a lattice architecture, where N + 1 couplers with coupling ratios (κ_0,..., κ_n) are needed for a N-AMZI filter. The AMZI stages are also equipped by phase shifts (φ_1,..,φ_n) to set the filter at the targeted central frequency. In order to achieve passband flattening, two different differential path lengths are used [18]. The first AMZI of each stage has a path length difference equal to the smallest path length difference ΔL_1, while the following AMZIs have double path length difference (ΔL_2). The FSR of the multi-stage filter is defined by ΔL_1. The advantage of the AMZI -based filters is that they do not impose any limitation on the maximum supported FSR [17], making them an attractive choice for the FSR extension functionality. The AMZI filter with $f_{FSRlatt1}$=5.3334 GHz is shown in Fig 3(b). It has 3 AMZIs per stage, so that the transition band of the filter is sharp enough to suppress by at least 50 dB the information that appears after 2.6667 GHz from the targeted channel. LIC-SS waveguides are considered for implementation of the 2 stage/3 AMZI lattice filter, resulting in a arm length difference of ~3.69 cm and ~7.38 cm for the first and rest of AMZIs, respectively. The second lattice filter with $f_{FSRlatt2}$ =10.6668 GHz is shown in Fig. 3 (c), requiring 2 AMZIs per stage in order to suppress the parasitic signals appearing after 5.3334 GHz from the targeted channel.

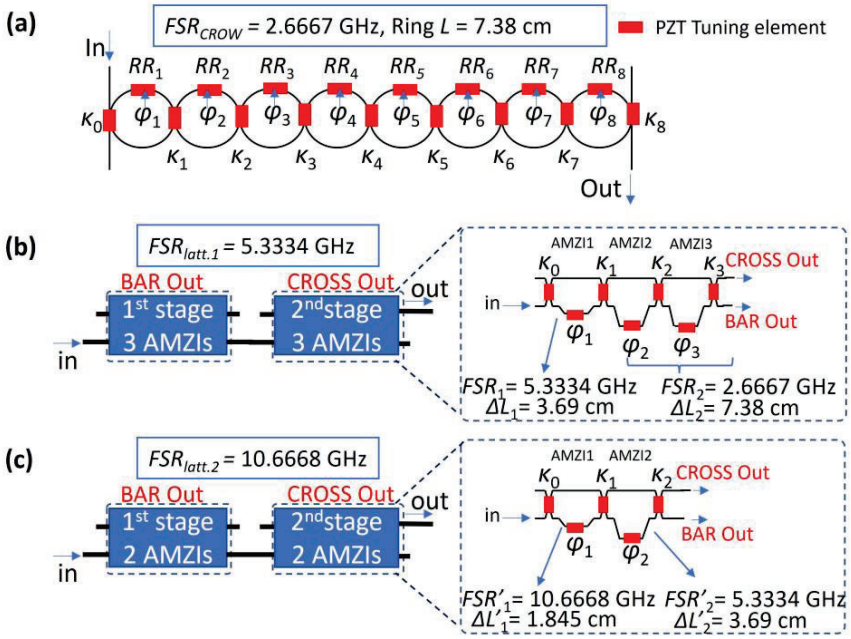

Figure 3. Individual filters of the channel selector chain: (a) 8- RR CROW filter with f_{FSR}=2.6667 GHz, (b) 2-stage/3 AMZI lattice filter with FSR=5.3334 GHz ($2\times f_{FSRCROW}$) and (c) 2-stage/2 AMZI lattice filter with FSR=10.6668GHz ($4\times f_{FSRCROW}$).

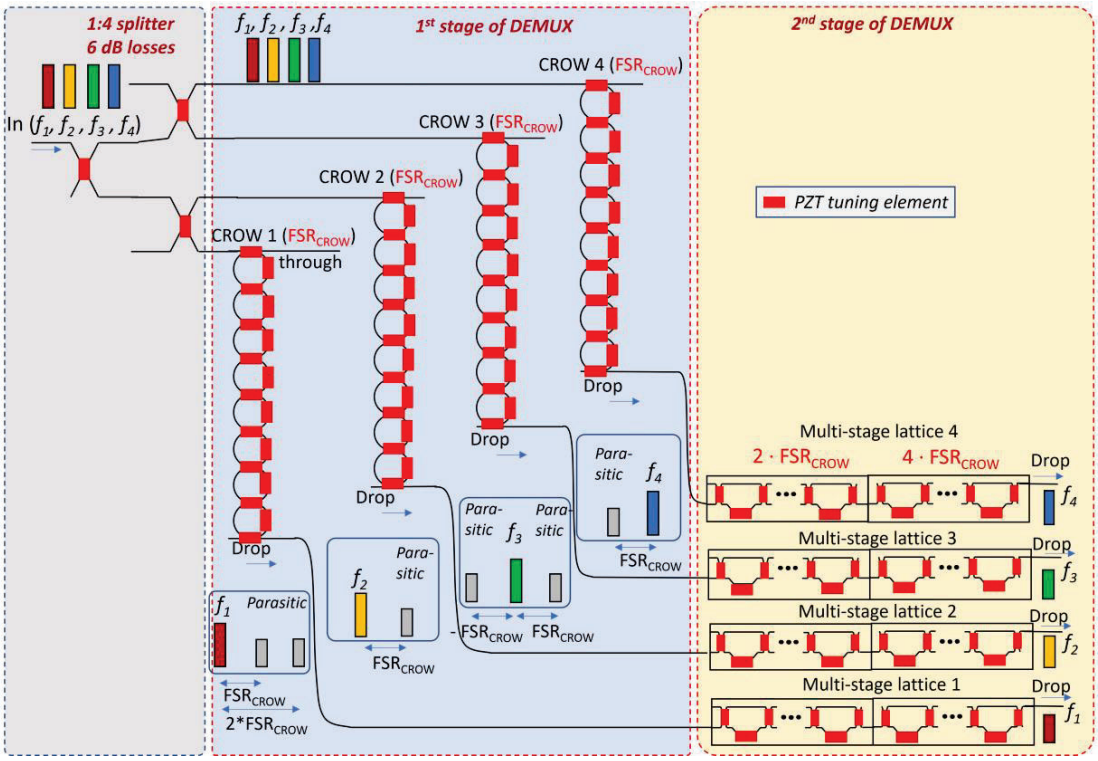

Figure 4. Four-channel photonic DEMUX circuit based on the nested Configuration with 1-to-4 optical splitter.

LIC-SS waveguides are assumed for the implementation of the 2 stage/ 2 AMZIs lattice filter, resulting in arm length differences of 1.845 cm and 3.69 cm for the first and second AMZI, respectively. Comparing the two AMZI lattice filters, it can be observed that the last lattice filter has 1 AMZI unit less. The parasitic signal to be suppressed by this filter is positioned further away and therefore its transition band can be less sharper. The number of PZT actuators of the FSR extender filter is equal to 24, resulting on a total number of 41 PZT actuators (=24+17) per channel selector filter.

From the single channel selector, a 4-channel DEMUX filter can be obtained by the proposed circuit topology shown in Fig. 4. This system employs an 1-to-4 tunable optical splitter which is responsible for splitting the incoming USB 4-channel signals (f_1, f_2, f_3, f_4) to 4 independent and identical paths. The splitter is implemented with tunable couplers allowing any splitting ratio between 1 and ¼. Each output of the splitter is connected to an identical 2-stage reconfigurable channel selector whose circuit is identical to the one described in Fig. 2 and 3. Specifically, the architecture consists of four identical CROW filters with $f_{FSRCROW}$= 2.6667 GHz, four 2 stage/ 3 AMZI lattice filters with $f_{FSRlatt1}$=5.3334 GHz and four 2 stage/ 2 AMZI lattice filters with $f_{FSRlatt2}$=10.6668 GHz. Each chain of those filters can be tuned to drop any of the channels (f_1, f_2, f_3, f_4). Since the 4 paths that enter each channel selector are independent, there is no restriction on the selected channel spacing. The proposed topologies provides high reconfigurability in terms of channel BW, channel spacing, central frequency and band operation (Ka-, Q- and V-band).

4. SIMULATION RESULTS

Fig. 5 presents the spectral response of each filter of the channel selector chain, separately. The commercially available software VPI Photonics is used to implement and simulate the filters [19]. The filters in the sub-figures are aligned on their central frequency in such a way that first passband of all filters is tuned to the same central frequency, the stopband of the AMZI lattice filters with $f_{FSRlatt1}$ and $f_{FSRlatt2}$ are tuned at the first and second repetition of the CROW's passband, respectively. For all filters, we assume the typical LIC-SS waveguide propagation losses of 1.5 dB/m as reported in [14].

In all graphs, the x-axis represents the relative optical frequency with respect to the optical carrier frequency. In the presented case study, it has been chosen to be between 42.5 GHz and 50 GHz, since by optically selecting a channel in this range will result in a RF channel at the V-band after beating of the optical carrier and the channel selector output in the PD.

Fig. 5 (a) presents the power spectral response of the CROW filter when tuned to exhibit the minimum targeted passband BW of 125 MHz and the maximum BW of 1000 MHz. The bandwidth of the CROW filter can be varied by changing the power coupling coefficients κ_n. The coupling coefficients settings for the minimum and maximum targeted BW are listed in Table 1 for 2 different waveguide propagation loss cases. All phase shifts are set to 0° in order to tune the filter to a specific central frequency (f_c). The largest difference in performance is exhibited for these 2 outer bandwidth values. Thus, by confirming that all the performance metrics (power ripple <1 dB, group delay variation < 5 ps, isolation > 40 dB) are met for the minimum and maximum BW, automatically means that the specifications are met also for any intermediate targeted BW. Analyzing, the passband of the CROW filter for the BW of 125 MHz, the maximum Insertion Loss (IL) and the power ripple at the Pass Band (PB) are equal to 3.8 dB and 0.84 dB respectively. As PB is considered to be the spectral area of $f_c \pm 0.5\times$BW. The respective IL and IL ripple for the BW of 1000 MHz are equal to 0.75 dB and 0.38 dB.

Figs. 5 (b) and (c) show the power spectral responses of the 2 stage/ 3 AMZI and the 2 stage/ 2 AMZI lattice filters, respectively. The coupling coefficients and phase shifts values of these two lattice filters can be found in Table 2. As it can be seen, the stopband level of both AMZI lattice filters is around 50 dB. By analyzing the passband of the lattice filters with $f_{FSRlatt1}$=5.3334 GHz and $f_{FSRlatt2}$=10.6668 GHz, we found that the IL at the PB are equal to 0.78 dB and 0.46 dB, respectively. The IL and group delay ripples for both AMZI lattice filters are negligible.

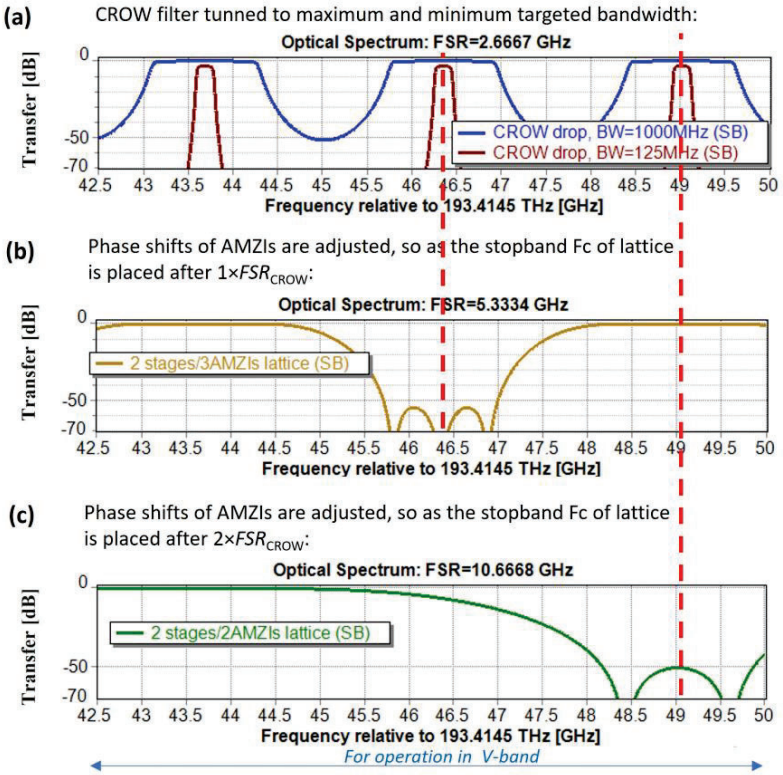

Figure 5. Simulated spectral response of the filters employed in the channel selector cascade: (a) 8-RR CROW filter with $f_{FSRCROW}$=2.6667 GHz tuned to exhibit a bandwidth of 125 MHz and 1000 MHz, (b) 2-stage/ 3 AMZI lattice filter with $f_{FSRlatt1}$ = 5.3334 GHz ($2\times f_{FSRCROW}$) and (c) 2-stage/ 2 AMZI lattice filter with FSR=10.6668 GHz ($4\times f_{FSRCROW}$).

Table 1. Optimized circuit parameters for a maximally flattened CROW bandpass filter with BW equal to 125 MHz and 1000 MHz. For each bandwidth, the values are given for the ideal lossless case and for the case that the propagation losses are equal to 1.5 dB/m. The values have been calculated via [17].

Parameter for CROW	**BW = 125 MHz**		**BW=1000 MHz**	
	Ideal Lossless waveguide	**SS waveguide L =1.5 dB/m**	**Ideal Lossless waveguide**	**SS waveguide L =1.5 dB/m**
κ_0, κ_8	0.34	0.35	0.907	0.907
κ_1, κ_7	0.0245	0.0315	0.655	0.655
κ_2, κ_6	0.011	0.016	0.505	0.505
κ_3, κ_5	0.009	0.015	0.438	0.44
κ_4	0.0085	0.0095	0.435	0.437
φ_1 to φ_8	0°	0°	0°	0°

Table 2. Optimized circuit parameters for a maximally flattened 3-AMZI and 2-AMZI lattice filters. The values have been calculated via [17].

Parameter for lattice filters	**Each stage of 3 AMZIs FSR_{latt1} = 5.3334 GHz SS waveguide, L=1.5 dB/m**	**Each stage of 2 AMZIs FSR_{latt2} = 10.6668 GHz SS waveguide, L=1.5 dB/m**
κ_0	0.5	0.5
κ_1	0.794	0.7143
κ_2	0.195	0.075
κ_3	0.0203	-
φ_1: 1st stage	0°	0°
φ_1: 2nd stage	180°	180°
φ_2 (both stages)	180°	180°
φ_3 (both stages)	180°	-

Next, the full architecture depicted in Fig. 4, is simulated. Since each channel is processed independently from an identical chain of filters, all channels exhibit the same spectral response in terms of IL, group delay and isolation performance. The only difference is that each channel is tuned to a different central frequency using the phase shifts. In this respect and without loss of generality, simulation results are presented for one of the channels. Particularly, Fig. 6 presents the spectral response of one channel selector during the different stages of filtering for the minimum targeted BW of 125 MHz. The spectral response after an optical impulse signal has passed through the 1:4 splitter and the CROW filter is presented in the first graph. The loss at the CROW filter output is equal to 9.8 dB at the passband, where the 1:4 splitter contributes by 6 dB and the CROW filter by 3.8 dB. Typical SS waveguide propagation losses of 1.5 dB/m have been considered. Three passbands appear in a BW of 7.5 GHz with distances between the 1st and 2nd passband being equal to 2.6667 GHz ($1\times f_{FSRCROW}$) and between the 1st and 3rd PB being equal to 5.3334 GHz ($2\times f_{FSRCROW}$).

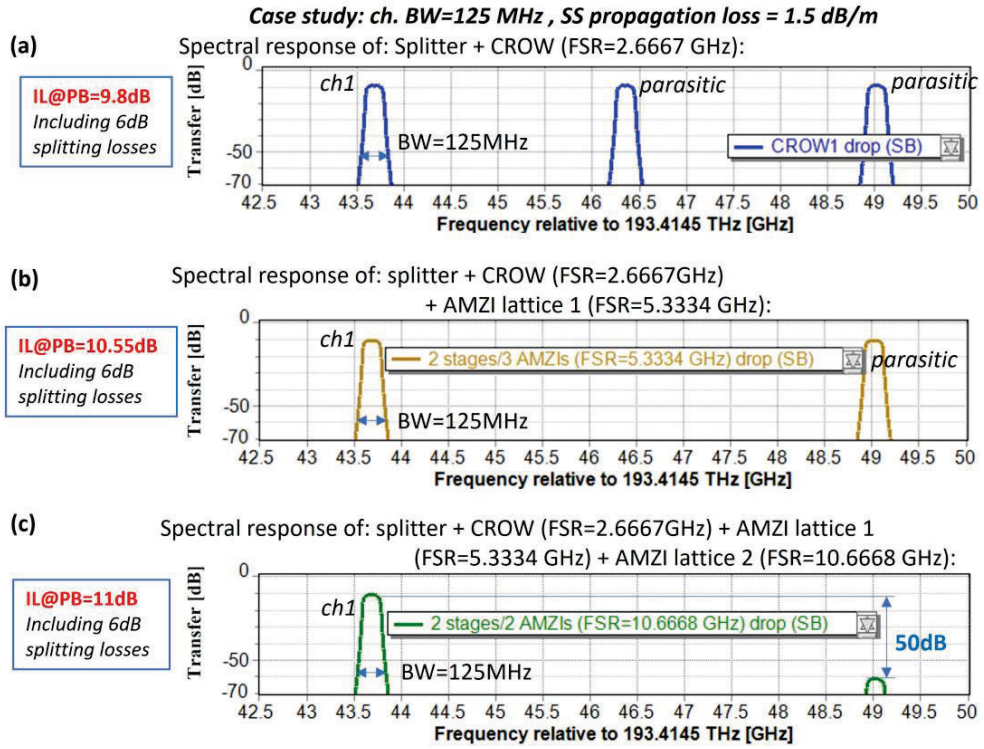

Figure 6. Demonstration of the channel selection for the case study that the channel bandwidth is set the minimum targeted value of 125 MHz. The displayed Insertion Loss (IL) at the Pass-Band (PB) correspond to typical propagation loss in Single Stripe equal to 1.5 dB/m.

Next, the signal is fed to the 2 stage/ 3 AMZI lattice filter with $f_{FSRlatt1} = 2 \times f_{FSRCROW}$ that is adjusted to suppress the 2nd PB. As it can be seen in Fig. 6 (b), the 2nd PB at the output of the AMZI lattice#1 filter is suppressed by more than 50 dB. The total losses at the PB of the remaining passbands are equal to 10.55 dB. Finally, the signal is sent to the 2 stage/ 2 AMZI lattice#2 filter with $f_{FSRlatt2} = 4 \times f_{FSRCROW}$, adjusted to suppress the 3rd PB. At the output of this filter only the 1st targeted PB appears, while the 3rd passband has been suppressed by 50 dB. The calculated total losses of the channel selector is 11 dB, including the 6 dB splitting losses. The total filtering loss of 5 dB is due to the assumed LIC-SS waveguide propagation loss of 1.5 dB/m. This value corresponds to the maximum losses that the channel selector exhibits when tuned over the full BW range of [125 -1000] MHz.

Figure 7 presents the respective results for the maximum channel BW of 1000 MHz and SS propagation losses of 1.5 dB/m. The losses of the channel selector at the final stage are equal to ~8 dB (6 dB splitting losses + 2 dB filtering losses), which are 3 dB smaller than in the case that the channel selector is tuned to the minimum BW of 125 MHz. Since the AMZI lattice filters have fixed passband BW and IL performance for any targeted channel BW, this 3 dB difference is stemming explicitly from the CROW filter, which serves as the BW regulator and exhibits highest losses when tuned to the smallest channel BW. In terms of channel isolation, the channel selector is able to suppress the 2nd and 3rd passbands by at least 50 dB, resulting on the targeted selection of a single channel-passband within a BW of 7.5 GHz.

The above analysis proves that for the typical LIC-SS waveguide propagation loss of 1.5 dB/m, any parasitic signal within the Ka-, Q- and V-band is suppressed more than 50 dB. Moreover, since the AMZI-lattice filters have negligible impact on the channel's passband flatness, the IL and group delay ripples depend only on the CROW filter response. Fig. 8 (a) and (b) show the power and group delay spectral response of the channel selector PB for the case that the CROW filter is tuned to the minimum BW of 125 MHz. The PB response is simulated for 2 cases: the ideal case that the waveguide propagation loss is 0 dB/m and for the case that SS waveguide exhibits typical propagation loss of 1.5 dB/m.

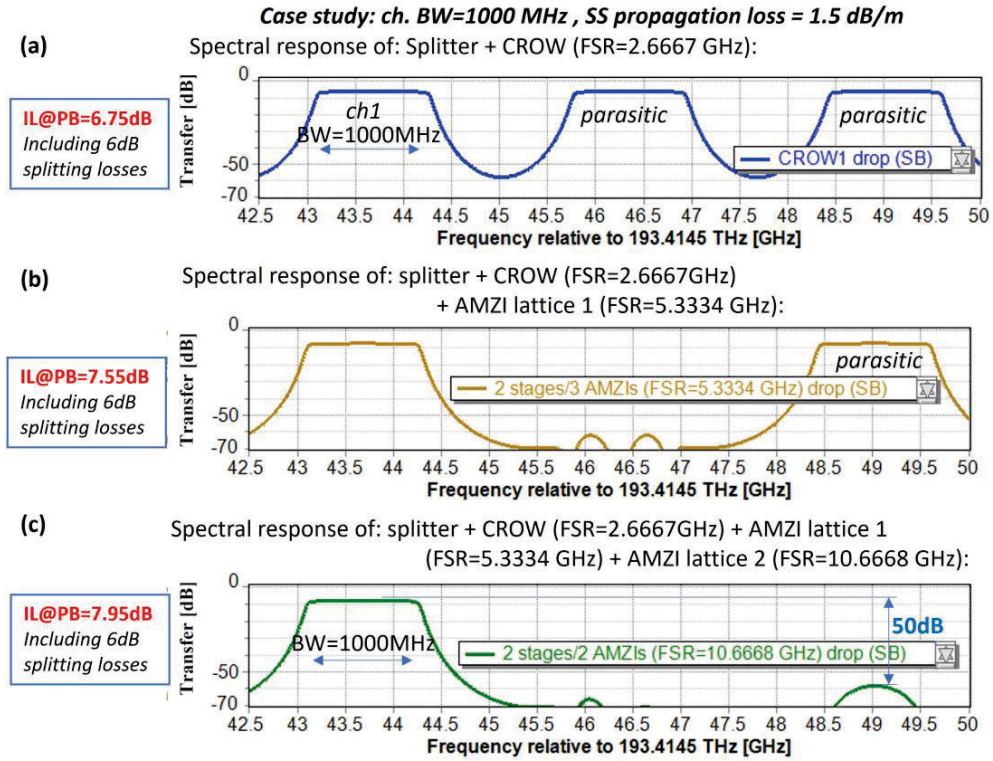

Figure 7. Demonstration of the channel selection for the case study that the channel bandwidth is set at the maximum targeted value of 1000 MHz. The displayed Insertion Loss (IL) at the PB corresponds to typical propagation loss in SS equal to 1.5 dB/m.

The tunning settings for both cases are given in Table 1. As it can be seen in the Table, the coupling coefficients for the lossy case are set to higher values with respect to the lossless case in order to compensate for the propagation loss,. This is because the introduction of loss decreases the PB width [17] and the use of slightly higher κ's brings it back to the targeted BW. For the ideal lossless case, shown in Fig. 8 (a), the IL at the PB is equal to 6 dB which corresponds to the splitting losses of the 1:4 optical splitter, while the IL introduced by the CROW and AMZI based-lattice filters is zero. When the propagation loss increases to 1.5 dB/m, then the IL at the edges of the PB is equal to 11 dB (6 dB splitting loss, 5 dB filtering loss) and the IL ripple within the BW range is equal to 0.84 dB. Considering the group delay response, shown in Fig. 8 (b), the presence of propagation loss has positive effect, since in the lossy case the group delay is less dispersive. For the range of $f_c \pm 0.5 \times BW$, the group delay ripples are equal to 6.3 ns and 2.8 ns for waveguide propagation loss of 0 dB/m and 1.5 dB/m, respectively.

Fig. 9 (a) and (b) depict the power and spectral response of the channel selector's PB for the case that the CROW filter is tunned to the maximum BW of 1000 MHz. The difference in performance between the lossless and lossy case is smaller for this BW. The IL at the edges of the PB is equal to 6 dB (only splitting losses) and 7.95 dB (6 dB splitting losses, 1.95 filtering losses) for propagation losses of 0 dB/m and 1.5 dB/m, respectively. The IL and group delay ripple for the lossy case is equal to 0.38 dB and 0.9 ns, respectively. By comparing Fig. 8 and Fig. 9, it can be noted that the channel selector exhibits the worst performance in terms of IL, IL and group delay ripple when the CROW filter is tuned to the smallest BW. This result can be explained from the fact that in order to adjust the filter to the minimum BW, the coupling coefficient are set to relatively small values. Small coupling coefficient values result on high-Q resonators and, thus, larger IL and group delay dispersion. Therefore, the performance of the channel selector filter is dictated by the minimum BW configuration, exhibiting an IL of 11 dB, an IL ripple of 0.84 dB and a group delay ripple of 2.8 ns at the spectral area of $f_c \pm 0.5 \times BW$.

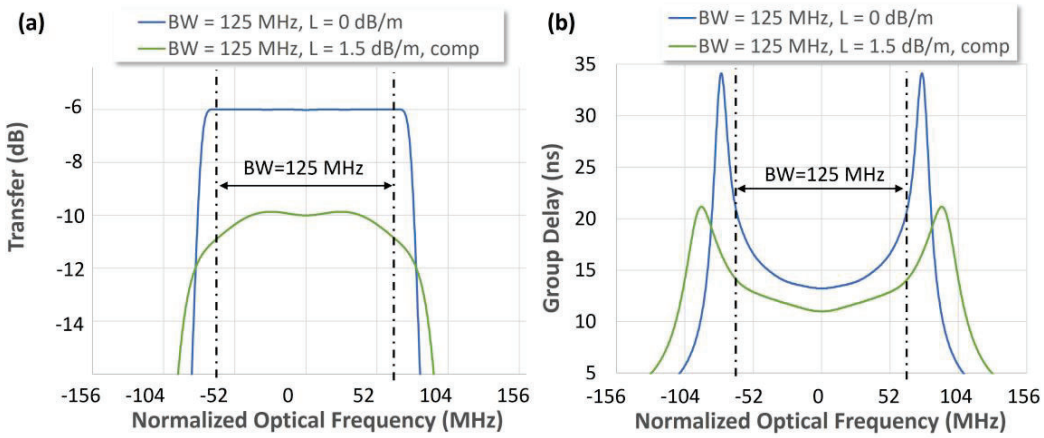

Figure 8. Spectral response at the output of the channel selector for BW = 125 MHz: (a) Power response, (b) group delay response. The spectral responses have been simulated for the implementation of the filter with ideal lossless waveguides (L=0 dB/m) and with TriPleX® LIC-SS typical waveguides loss (1.5 dB/m).

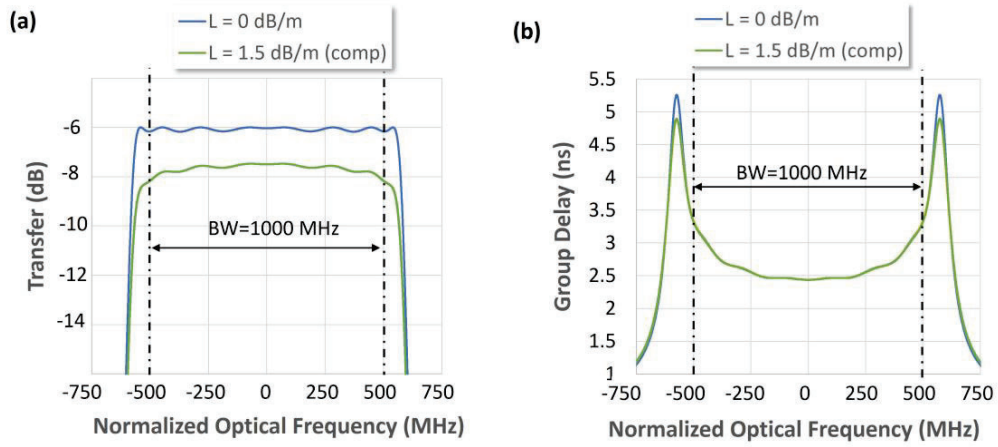

Figure 9. Spectral response at the output of the channel selector for BW = 1000 MHz: (a) Power response, (b) group delay response. The spectral responses have been simulated for the implementation of the filter with ideal lossless waveguides (L=0 dB/m) and with TriPleX® LIC-SS typical waveguides loss (1.5 dB/m).

5. OUTLOOK

Our vison is to realize the proposed RF_{in}-to-RF_{out} DEMUX architecture (see Fig.1) into the hybrid InP-TriPleX® iMWP platform [13], providing also the necessary RF signal interfaces. A combination of 2 different photonics platforms will be utilized to get the best performance of every building block of the architecture. The active components for the light generation and electrical-optical-electrical (E-O-E) conversion will be implemented in the Indium Phosphide (InP) platform [20]. InP is a III-V semiconductor material that has excellent electro-optic properties making it suitable for the fabrication of high speed modulators and detectors, as well as optical gain sections. However, InP exhibits high propagation losses (2 dB/cm), prohibiting its use for advanced filtering/processing functionalities. Thus, for the processing unit, which consists of the splitters and filters, the Si_3N_4/SiO_2 optical waveguide platform known as TriPleX®

is going to be used [13], [14]. The passive Si_3N_4/SiO_2 waveguides offer ultra-low propagation loss which is critical for the high-Q channel selection filtering operation.

As an example, Fig. 10 presents a 3D render of one of our recent hybrid iMWP modules. The module has been designed to enable satellite beamforming functionalities for the H2020 project "SpaceBeam" [21]. The respective fabricated iMWP module is presented in Fig. 11. In the middle of the module is located the TriPleX® processing unit, having multiple interfaces to: a gain section used for lasing, 2 arrays of MZMs, an array of PDs and 2 fiber arrays. The fiber arrays are employed for initial calibration of the module. Except for the optical interfaces, the DC and RF electrical interfacing is performed via gold wire bonds that are connected to separate printed circuit boards (PCBs). As shown in Fig. 11, the hybrid assembly is mounted on a gold plated copper base, which holds the PCBs, the PICs, and provides support for the fiber arrays.

Utilizing the same hybrid integration approach, we aim to realize the proposed DEMUX architecture shown in Fig. 1. The target is to manufacture a system with improved Size, Weight and Power consumption (SWaP) envelope with respect to the current RF solutions. Additional advantages stemming from the integration of the architecture in the hybrid iMWP platform is the fully reconfigurability of the system by means of low-power consumption stress-optic PZT tuning elements and the inherent Electro-Magnetic Interference (EMI) shielding, provided by the guidance of the signal into the crosstalk-free optical waveguides. All these advantages establish a flexible and robust hardware platform that can be a highly attractive solution of the targeted field of satellite communications.

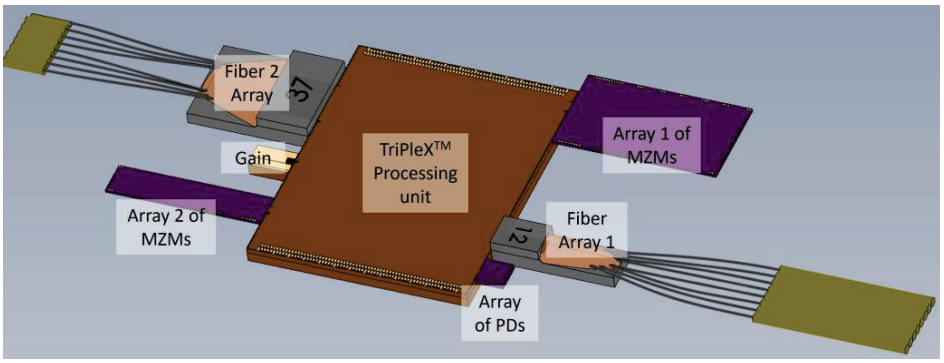

Figure 10. 3D render example of a state-of-the art hybrid InP-TriPleX® iMWP module [21] that consists of: TriPleX® Si_3N_4/SiO_2 processing unit on the center, 2 fiber arrays, an InP gain section (laser), 2 arrays of Mach-Zehnder Modulators (MZMs) and an array of Photo-Diodes (PDs).

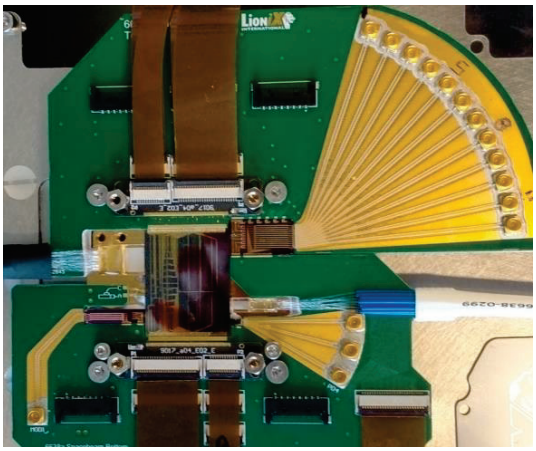

Figure 11. Photograph of a state-of-the-art assembled iMWP module which is hybrid integrated by LioniX International [21].

6. CONCLUSION

In this paper, we presented a photonic channel selector filter design that allows for fully reconfigurable central frequency and channel BW simultaneously in the Ka, Q and V-band. The proposed channel selector filter has a FSR of 10.6668 GHz and consists of 2 stages of filtering. The first stage of filtering is based on a CROW filter, which considered to be the key building block of the architecture, serving as the channel central frequency selector and BW regulator. The second stage of filtering consists of AMZI-lattice filters and serves as FSR extender. Moving from the single channel selector to the 4-channel DEMUX system, we proposed a nested configuration that incorporates an 1-to-4 optical splitter in order to allow for maximum flexibility in terms of channel BW, channel spacing, central frequency and frequency band operation. The tuning strategy involves biasing of multiple low power consumption PZT actuators, simultaneously. By properly configuring the PZT tuning elements the filter exhibits in worst case an IL of 11 dB (6 dB splitting losses, 5 dB filtering losses), an IL ripple of 0.84 dB and a group delay ripple of 2.8 ns, while the isolation between the adjacent channels is larger than 50 dB. It is important to highlight that realizing such a performance has been possible only because of the very low waveguide loss, provided by the single stripe Si_3N_4/SiO_2 TriPleX® waveguide technology.

ACKNOWLEDGMENT

This work has been supported by the European Space Agency (ESA) within the program “Photonic RF Tuneable Demultiplexer for Broadband Satellites - THORMUX”, Contract no. 4000134602/21/NL/AR and by H2020 within the program “SpaceBeam”, Contract no. 870421.

REFERENCES

[1] Capmany, J. and Novak, D., “Microwave photonics combines two worlds,” Nat. Photon. 1, 319–30 (2007).
[2] Seeds, A.J. and Williams, K. J., “Microwave photonics,” J. of Light. Tech., 4628–41 (2006).
[3] Marpaung D., Yao J., et al., "Integrated Microwave Photonics." Nature Photonics 13, 80-90 (2019).
[4] Piqueras M. A., et al, "Tunable and reconfigurable photonic Rf filtering for flexible payloads," Proc. SPIE 10562, Int. Conf. on Space Optics, ICSO 2016, 1056220 (2017).
[5] Choudhary A., et al., “Advanced integrated microwave signal processing with giant on-chip Brillouin gain,” J. Lightwave Technol. 35, 846–854 (2017).
[6] Li Z., et al., “A Reconfigurable Microwave Photonic Channelized Receiver Based on Dense Wavelength Division Multiplexing Using an Optical Comb,” Opt. Commun. 285 (9), (2012).
[7] J. Yao, “Photonics to the Rescue: A Fresh Look at Microwave Photonic Filters,” in IEEE Microwave Mag. 16 (8), 46-60 (2015).
[8] Zhang, W., Yao, J. “A fully reconfigurable waveguide Bragg grating for programmable photonic signal processing,” Nat Commun 9, 1396 (2018).
[9] Deng, X., et al. “Polarization-insensitive and tunable silicon Mach-Zehnder wavelength filters with flat transmission passband” IEEE Phot. J. (2018).
[10] Zhuang L., “Flexible RF filter using a nonuniform SCISSOR,” Opt. Lett. 41 (6), 1118–1121 (2016).
[11] Liu Y., et al., “Integrated microwave photonic filters,” Advances in Opt. and Phot.12, 485-555 (2020).
[12] Gómez-García R., et al., “High-Order Planar Bandpass Filters With Electronically-Reconfigurable Passband Width and Flatness Based on Adaptive Multi-Resonator Cascades,” IEEE Access 7, 11010-11019 (2019).
[13] Roeloffzen C. G. H., et al., “Low-Loss Si3N4 TriPleX Optical Waveguides: Technology and Applications Overview,” IEEE J. of Sel. Top. in Quant. Electr. 24 (4), 1-21 (2018).
[14] Taddei C., et a., “High-Selectivity On-Chip Optical Bandpass Filter With Sub-100-MHz Flat-Top and Under-2 Shape Factor,” IEEE Phot. Techn. Lett. 31 (6), 455-458, (2019).
[15] Everhardt A. S., et al., “Ultra-low power stress-based phase actuation in TriPleX photonic circuits,” in Proc. SPIE-WEST, 1200405 (2022).
[16] J. Yao, “Microwave photonics: Photonic generation of microwave and millimeter-wave signals,” Int. J. Microw. Opt. Technol. 5 (1), (2010).

[17] Madsen C. K., and Zhao J. H., "Optical Filter Design and Analysis: A Signal Processing Approach," online Wiley book, Online ISBN:9780471213758 (1999).
[18] Liu T., Soh Y. C. ,Zhang Y., and Fang Z., "Parameter optimization of an all-fiber Fourier filter flat-top interleaver," Opt. Eng. 41, 3217-3220 (2002).
[19] https://www.vpiphotonics.com/index.php
[20] Zhou G., et al., "High-Power InP-Based Waveguide Integrated Modified Uni-Traveling-Carrier Photodiodes," J. Lightwave Technol. 35, 717-721 (2017).
[21] https://www.spacebeam-project.eu/project/